# Structure and Function of a Dehydrating Condensation Domain in Nonribosomal Peptide Biosynthesis

Jon B. Patteson[a^], Camille Marie Fortinez[b^], Andrew T. Putz[a], Juan Rodriguez-Rivas[c], L. Henry Bryant III[a], Kamal Adhikari[b], Martin Weigt[c], T. Martin Schmeing[b*], Bo Li[a*]

[a]Department of Chemistry, The University of North Carolina at Chapel Hill, Chapel Hill, NC 27599, United States

[b]Department of Biochemistry and Centre de recherche en biologie structurale, McGill University, Montréal, Canada H3G 0B1

[c]Sorbonne Université, CNRS, Institut de Biologie Paris-Seine, Laboratory of Computational and Quantitative Biology, Paris, France 75005

^These authors contributed equally to this work.

*To whom correspondence may be addressed

**Email:** boli@email.unc.edu, martin.schmeing@mcgill.ca

**Keywords (3 to 5):** biosynthesis | dehydration | nonribosomal peptide synthetase | condensation

**This PDF file includes:**

Main text
Figures 1 to 6
Table of content figure

**Abstract**

Dehydroamino acids are important structural motifs and biosynthetic intermediates for natural products. Many bioactive natural products of nonribosomal origin contain dehydroamino acids; however, the biosynthesis of dehydroamino acids in most nonribosomal peptides is not well understood. Here, we provide biochemical and bioinformatic evidence in support of the role of a unique class of condensation domains in dehydration ($C_{modAA}$). We also obtain the crystal structure of a $C_{modAA}$ domain, which is part of the nonribosomal peptide synthetase AmbE in the biosynthesis of the antibiotic methoxyvinylglycine. Biochemical analysis reveals that AmbE-$C_{modAA}$ modifies a peptide substrate that is attached to the donor carrier protein. Mutational studies of AmbE-$C_{modAA}$ identify several key residues for activity, including four residues that are mostly conserved in the $C_{modAA}$ subfamily. Alanine mutation of these conserved residues either significantly increases or decreases AmbE activity. AmbE exhibits a dimeric conformation, which is uncommon and could enable transfer of an intermediate between different protomers. Our discovery highlights a central dehydrating function for $C_{modAA}$ domains that unifies dehydroamino acid biosynthesis in diverse nonribosomal peptide pathways. Our work also begins to shed light on the mechanism of $C_{modAA}$ domains. Understanding $C_{modAA}$ domain function may facilitate identification of new natural products that contain dehydroamino acids and enable engineering of dehydroamino acids into nonribosomal peptides.

**Main Text**

**Introduction**

Dehydroamino acids occur in many bioactive natural products, such as the antibiotic nisin, the anticancer drug romidepsin (Istodax), and the cyanobacterial toxin microcystin-LR (Figure S1A).[1-3] These noncanonical amino acids provide natural products with conformational rigidity, proteolytic stability, and reactive functionalities that facilitate interactions with their biological targets.[4] For example, the α,β-dehydroalanine (Dha) in microcystin-LR forms a covalent linkage with a nucleophic cysteine in the target.[5] In addition, the unique electronic properties and chemical reactivities of α,β-dehydroamino acids enable them to participate in diverse chemical transformations, including nucleophilic-, radical-, and cyclo-additions in biomolecules under mild conditions.[6] Biosynthesis of dehydroamino acids has been extensively studied in ribosomally synthesized and posttranslationally modified peptide (RiPP) natural products, such as nisin, whereby Dha and dehydrobutyrine (Dhb) are installed by lanthipeptide dehydratases via dehydration of serine and threonine, respectively.[7] Dha/Dhb can subsequently be converted to lanthionines, lysinoalanines, pyridines, and to D-amino acids in RiPP biosynthesis, which highlights the versatility of dehydroamino acid intermediates in biosynthetic transformations.[8]

Many nonribosomal peptides contain dehydroamino acids, such as the aforementioned romidepsin and microcystin-LR (Figure S1A),[2-3] or are hypothesized to be derived from dehydroamino acid intermediates, such as the antitumor drug bleomycin and azabicyclene (Figure S1B).[9-10] Nonribosomal peptides are a major class of natural products that exhibit wide-ranging biological activities and therapeutic applications. The biosynthesis of nonribosomal peptides requires nonribosomal peptide synthetases (NRPSs), assembly lines made up of repeating sets of domains that organize into modules.[11-12] A typical module contains an adenylation (A) domain that activates an amino acid, a thiolation (T) domain where the amino acid is tethered via a thioester, and a condensation (C) domain that forms an amide bond between the amino acids on the donor and acceptor T domains. Once peptide elongation completes, a terminal thioesterase (TE) domain cleaves the thioester, which releases the free peptide from the T domain. Using this assembly line strategy with assistance from tailoring enzymes, NRPSs bypass the ribosome and incorporate nonproteinogenic amino acids into nonribosomal peptides at different stages of biosynthesis, including directly activating the nonproteinogenic amino acid using the A domain, modifying the amino acid after its loading onto a T domain, or modifying the amino acid on a peptide product. The enamine of dehydroamino acids is unstable and prone to hydrolysis, therefore, the biosynthesis of Dha or Dhb in bleomycin,

mycrocystin-LR, and syringomycin was proposed in the 2000s to involve dehydration of serine or threonine tethered to a T domain on the NRPS assembly line.[3, 9, 13-14] However, the timing of dehydration was unclear (*i.e.* whether dehydration occurs on a T domain-tethered amino acid or a tethered peptide). It was also unknown whether an NRPS domain or an auxillary tailoring enzyme is responsible for dehydration.

A phylogenetic study of C domains in 2012 showed that two C domains of the bleomycin NRPSs and a C domain of the microcystin-LR NRPS form a distinct clade from the other C domains.[15] These C domains were proposed to participate in modifying the amino acid incorporated on the NRPS assembly line, and were assigned the name "modified AA" (modAA). We will refer to these C domains as $C_{modAA}$. Our expanded bioinformatic analysis found that $C_{modAA}$ domains also exist in NRPSs involved in the biosynthesis of other nonribosomal peptides that contain dehydroamino acids or are likely derived from dehydroamino acid intermediates.[16] Despite the compelling bioinformatic evidence for a role of $C_{modAA}$ domain in dehydration, no experimental evidence existed to support this function until very recently in the nonribosomal peptide albopeptide, which contains two consecutive Dha and Dhb.[17] *In vitro* reconstitution of the NRPS, AlbB, in albopeptide biosynthesis confirmed the function of two AlbB-$C_{modAA}$ domains in the dehydration of Ser and Thr to generate Dha and Dhb, respectively. Although this study provided important biochemical evidence for the function of $C_{modAA}$ domains, no structural information of $C_{modAA}$ domains was available and mechanistic understanding of $C_{modAA}$ domains was also lacking.

Notably, a C domain in nocardicin biosynthesis, NocB-$C_5$, also generates a dehydroamino acid intermediate and uses this intermediate to synthesize the β-lactam ring in nocardicin.[18-19] NocB-$C_5$ appears to be a unique member of the $^{D}C_{L}$ subfamily of C domains that typically catalyze condensation between a D- and an L-amino acid. The $^{D}C_{L}$ subfamily is distinct from $C_{modAA}$ domains, which is a different way to introduce dehydroamino acids by NRPSs. While detailed mutational analysis of NocB-$C_5$ has identified key residues for activity, the divergence in sequence of NocB-$C_5$ from $C_{modAA}$ domains (Figure S2A) suggests that different residues may be required for the activity of $C_{modAA}$ domains.

We identified a $C_{modAA}$ domain in the biosynthesis of methoxyvinylglycine or L-2-amino-4-methoxy-*trans*-3-butenoic acid (AMB, Figure 1A), an antimicrobial nonproteinogenic amino acid produced by *Pseudomonas aeruginosa* that arrests plant seed germination.[16, 20] AMB is produced as an alanyl-AMB dipeptide (Ala-AMB) by a NRPS pathway, which requires two NRPSs, AmbB and AmbE, and two non-heme iron, α-ketoglutarate-dependent oxygenases, AmbC and AmbD.[16] AmbB contains a typical domain order of A-T-C, which activates and loads alanine prior to using it as the donor in condensation. In contrast, AmbE's composition of Q-A-MT-$T_1$-$C_{modAA}$-$T_2$-TE is unusual in several aspects: it contains a domain of unknown function (Q domain) at the N terminus, and there is no A domain between the $C_{modAA}$ and $T_2$ in the final module, so two T domains directly flank $C_{modAA}$ (Figure 1B). The Q domain shares low sequence identity with X domains in vancomycin biosynthesis and interface (I) domains in siderophore biosynthesis (Figure S2B). AmbE activates and loads glutamate on $T_1$ followed by sequential hydroxylation by AmbC and AmbD, which produces a β,γ-dihydroxyglutamate intermediate linked to AmbE (Figure 1C).[16] Subsequently, a methyltransferase (MT) domain in AmbE catalyzes methylation of the γ-hydroxyl group and the C domain in AmbB condenses the modified glutamate with an alanine, which yields Ala-β-hydroxy-γ-methoxy-Glu (hereafter referred to as pre-Ala-AMB) (Figure 1C).[16] Characterization using deuterium-labeled glutamate as substrate revealed that the α-proton/deuterium is removed during the conversion from pre-Ala-AMB to Ala-AMB, which suggests that pre-Ala-AMB undergoes α,β-dehydration to a cryptic dehydroamino acid intermediate that enables decarboxylation to generate Ala-AMB (Figure 1C).[16] AmbE-$C_{modAA}$ belongs to the modAA subfamily of C domains (Figure 1D), and we proposed that AmbE-$C_{modAA}$ catalyzes the cryptic α,β-dehydration in the last steps of Ala-AMB biosynthesis.[16]

Here, we characterize the structure and function of the $C_{modAA}$ domain in AMB biosynthesis and provide experimental support for its role as a dehydrating condensation domain. We identified important residues of AmbE-$C_{modAA}$ for dehydrative decarboxylation by mutagenesis and studied the mutants under both multiple- and single- turnover conditions. We bioinformatically

analyzed 27 $C_{modAA}$ domains in biosynthetic pathways for known natural products and suggest that these $C_{modAA}$ domains are responsible for incorporating α,β-dehydroamino acids in these natural products that enable diverse biosynthetic transformations.

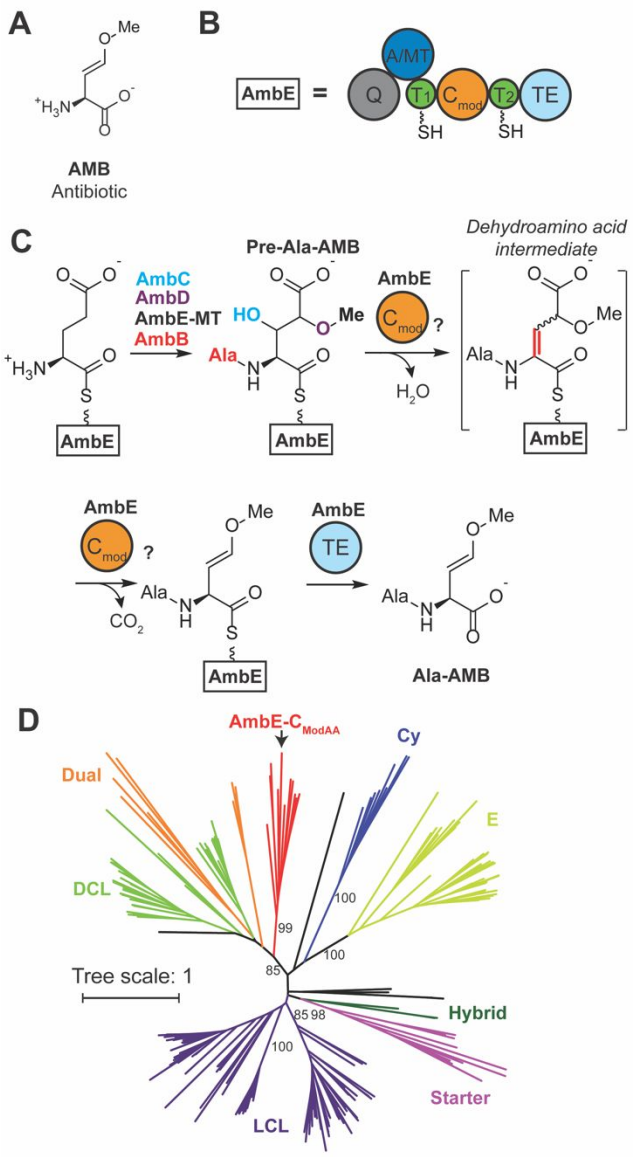


**Figure 1**. Identification of a condensation (C) domain that may catalyze dehydration in the synthesis of nonribosomal peptides. **A**) Structure of L-2-amino-4-methoxy-*trans*-3-butenoic acid (AMB). **B**) Domain organization of AmbE in colored spheres (A: adenylation, $C_{modAA}$: condensation with a role in modifying amino acids, MT: methyltransferase, T: thiolation, TE: thioesterase, Q: unknown function). The wavey line and SH indicates the phosphopantetheine (ppant) arm of T domains. **C**) Biosynthesis of Ala-AMB. A $C_{modAA}$ domain ($C_{mod}$ for short) is proposed to catalyze dehydration of pre-Ala-AMB to Ala-AMB that is tethered to the NRPS AmbE. **D**) Unrooted maximum likelihood phylogenetic tree of 199 C domains including 3 modAA domains from NaPDoS database and 9 other $C_{modAA}$ domains from known natural product pathways that are homologous to AmbE-$C_{modAA}$. These $C_{modAA}$ domains (red) form a unique subfamily of C domains. Tree scale represents

average expected percentage (1= 100%) of amino acid substitutions per site. Bootstrap values greater than 80 are labeled next to the branches. Abbreviations: LCL, condensation between two L-amino acids (purple); DCL, condensation between a D- and an L-amino acid (green); dual, condensation and epimerization (orange); starter, acylation to various molecules (pink); hybrid, condensation of amino acid to polyketide (dark green); Cy, condensation and heterocyclization (blue); E, epimerization (yellow). The sequences in black do not belong to any of these groups. The modAA clade contains $C_{modAA}$ domains from the following sequences: AmbE (AAG05690.1), AzeB (AAG06715.1, azabicyclene biosynthesis), DepE (ABP57749.1, romedepsin biosynthesis), BlmX (AAG02359.1, bleomycin biosynthesis), BlmVI (AAG02355.1, bleomycin biosynthesis), LgnD (AIZ66879.1, legonmycin biosynthesis), HasO (CZT62784.1, hassallidin biosynthesis), Zmn17 (CCM44337.1, zeamine biosynthesis), NdaA (ATP76243.1, nodularin biosynthesis), McyA (BAA83992.1, microcystin biosynthesis), PuwF (AIW82283.1, puwainaphycin biosynthesis), and PuwG (AIW82284.1, puwainaphycin biosynthesis).

## Results

### AmbE-$C_{modAA}$ transforms pre-Ala-AMB to Ala-AMB on the donor $T_1$ domain.

To characterize the function of the $C_{modAA}$ domain in AMB biosynthesis and determine if $C_{modAA}$ acts on its donor T ($T_1$) or acceptor T domain ($T_2$), we generated AmbE constructs containing different domain combinations. The TE domain was omitted to prevent release of the product from the T domains of the NRPSs. A one-pot reaction was performed including AmbB, AmbC, AmbD (AmbBCD hereafter), and different AmbE constructs in the presence of all necessary substrates and cofactors. Cysteamine was used in these one-pot reactions to capture the intermediates that accumulate on the NRPS and to probe thiotemplated biosynthesis (Figure S3).[16, 21] The captured cysteamine adducts were characterized using liquid chromatography-coupled high resolution mass spectrometry (LC-HRMS) (Figure 2). We expressed truncates of AmbE that ended before $C_{modAA}$ (Q-A-MT-$T_1$) or after $C_{modAA}$ (Q-A-MT-$T_1$-$C_{modAA}$). The one-pot reaction containing AmbE-Q-A-MT-$T_1$ and AmbBCD yielded captured pre-Ala-AMB (Figure S4B). Formation of pre-Ala-AMB without $C_{modAA}$ indicates that pre-Ala-AMB accumulates on $T_1$ prior to the action of $C_{modAA}$ (Figure 2). When Q-A-MT-$T_1$-$C_{modAA}$ was used in the reaction, captured Ala-AMB was detected (Figure 2B, S4, and S5). Results from these reactions suggest that $C_{modAA}$ transforms pre-Ala-AMB to Ala-AMB on the donor $T_1$ domain.

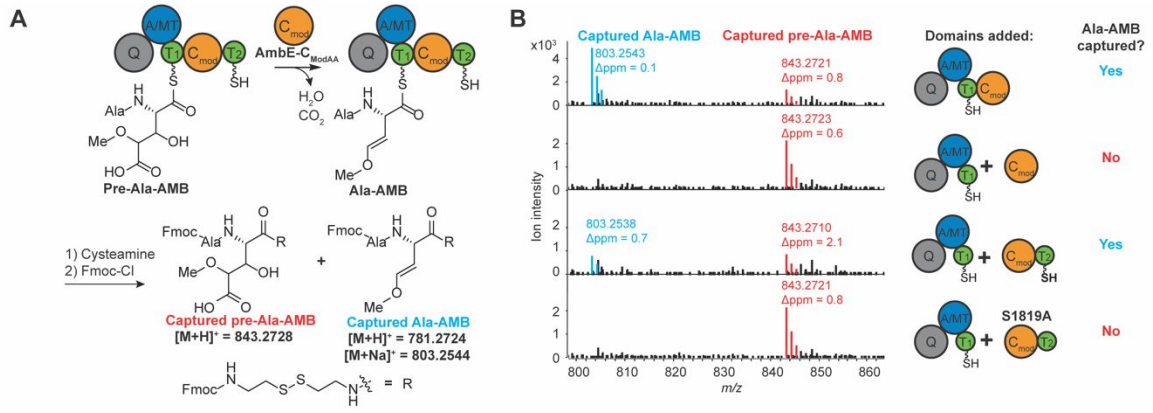


**Figure 2**. Transformation of pre-Ala-AMB to Ala-AMB requires $C_{modAA}$ *in cis* and $C_{modAA}$-$T_2$ *in trans*. **A**) One-pot reaction scheme. When different combinations of AmbE constructs are used instead of full length AmbE, late-stage biosynthetic intermediates accumulate on the T domains and are released and captured by cysteamine and detected by LC-HRMS. **B**) LC-HRMS analysis of captured pre-Ala-AMB or Ala-AMB (structures shown in **A**). A wider mass window that include

both $[M+H]^+$ and $[M+Na]^+$ ions for each compound is shown in Figure S4B. Δppm, parts per million error between the calculated and observed mass to charge ratios (*m*/*z*). Additional controls are shown in Figure S5. Ala-AMB formation requires attachment of $C_{modAA}$ to $T_1$ or *holo* $T_2$ in the split system. S1819A indicates an alanine mutation of the conserved serine in $T_2$ where the ppant arm is attached.

We also tested the activity of $C_{modAA}$ *in trans* by separating AmbE into Q-A-MT-$T_1$ and $C_{modAA}$-$T_2$. Incubation of $C_{modAA}$-$T_2$ with AmbBCD and Q-A-MT-$T_1$ in the one-pot reaction with cysteamine yields captured Ala-AMB, albeit at a lower level than Q-A-MT-$T_1$-$C_{modAA}$ (Figures 2B, S4, and S5). This result further supports the requirement of $C_{modAA}$ for the biosynthesis of Ala-AMB and demonstrates that the split system is functional for investigating $C_{modAA}$ activity. Truncation of $C_{modAA}$-$T_2$ to only include the $C_{modAA}$ domain in the reaction still resulted in similar levels of captured pre-Ala-AMB but no captured Ala-AMB (Figure 2B). This surprising result suggests that $T_2$ is required for Ala-AMB production in the split system when $C_{modAA}$ is separated from Q-A-MT-$T_1$. Additionally, mutation of the catalytic S1819 residue on $T_2$ to Ala in $C_{modAA}$-$T_2$ abolishes Ala-AMB formation. This mutation prevents the installment of the phosphopantetheine (ppant) arm on $T_2$. The lack of Ala-AMB formation by this mutant indicates that *holo* $T_2$ is needed for the split system to function (Figures 2B, S5). Together, these experiments reveal that pre-Ala-AMB is converted to Ala-AMB by $C_{modAA}$ while attached to $T_1$ and that $C_{modAA}$ must be part of a construct including the upstream module (Q-A-MT-$T_1$) or downstream domain (*holo* $T_2$) to be functional.

Because *holo* $T_2$ is required for the split system to function, we further examined the possibility that $C_{modAA}$ might convert pre-Ala-AMB to Ala-AMB on $T_2$ instead of $T_1$. We previously found that the full length AmbE $T_2$ mutant (S1819A) did not release free Ala-AMB in the one-pot reaction.[16] Adding cysteamine to this reaction only resulted in captured pre-Ala-AMB.[16] Although these results seemed to suggest formation of Ala-AMB might take place on $T_2$, reanalysis of the cysteamine capture data revealed that the S1819A mutant produces free Ala-AMB that is not linked to cysteamine (Figure S6). This unexpected result shows that the $T_2$ mutant is able to convert pre-Ala-AMB to Ala-AMB and supports the conclusion that $C_{modAA}$ modifies pre-Ala-AMB on $T_1$.

Production of free-Ala-AMB by the $T_2$ mutant may result from the action of the AmbE-TE domain, which could cleave cysteamine from the Ala-AMB-cysteamine adduct. Consistent with this proposal, adding cysteamine to the one-pot reaction of the AmbE TE mutant (S1956A) generated abundant cysteamine captured Ala-AMB, but little free Ala-AMB (Figure S6). Furthermore, adding cysteamine to the wildtype AmbE reaction also boosted the production of free Ala-AMB (Figure S6). Together, these data support a model in which *holo* $T_2$ is required for transfer of Ala-AMB and subsequent cleavage by TE in full length AmbE. In the split system, *holo* $T_2$ may help stabilize $C_{modAA}$ or facilitate interactions between $C_{modAA}$ and $T_1$.

**AmbE-$C_{modAA}$ transfers Ala-AMB to the acceptor $T_2$ domain.**

The split AmbE system was coupled with size exclusion chromatography to determine if Ala-AMB is transferred to the acceptor $T_2$ domain. Upon completion of a scaled-up one-pot reaction for Ala-AMB biosynthesis, Q-A-MT-$T_1$ and $C_{modAA}$-$T_2$ were separated by size exclusion chromatography (Figure S7), and the intermediates linked to Q-A-MT-$T_1$ and $C_{modAA}$-$T_2$ were captured by cysteamine. Pre-Ala-AMB was only detected on Q-A-MT-$T_1$, while Ala-AMB was detected on both Q-A-MT-$T_1$ and $C_{modAA}$-$T_2$ (Figure S7). This result supports that Ala-AMB is formed on $T_1$ and subsequently transferred to $T_2$. Detection of Ala-AMB on $T_1$ suggests that the transfer of Ala-AMB from $T_1$ to $T_2$ is less efficient in the split system than in full length AmbE.

**Crystallography of AmbE-$C_{modAA}$**

We conducted structural studies of AmbE-$C_{modAA}$ to further understand the activity of this domain. Purified $C_{modAA}$ was subject to crystallization screening and initial conditions were optimized to yield crystals suitable for diffraction. We obtained a 2.1 Å resolution structure of AmbE-$C_{modAA}$

with an $R_{free}$ of 23% (Table S2). Two copies of $C_{modAA}$ exist in the asymmetric unit in near-identical conformation. AmbE-$C_{modAA}$ possesses an overall structure similar to other proteins in the C domain family:[22] a V-shaped pseudodimer consisting of N- and C-terminal lobes with a chloramphenicol acetyltransferase (CAT) fold (Figure 3A). These lobes are known to exist in different relative orientation or "openness" in previously determined, catalytically active C domains, and AmbE-$C_{modAA}$ falls in the middle of this observed range (Figure S9A).[23-24] The junction of the lobes forms the classic active site tunnel that connects the canonical donor and acceptor T domain binding sites with the active site (Figure S9B), where the typical C domain HHXXXDG motif (H1496−G1502) is located (Figures 3A, S9B). Notably, the latch element (H1705−P1711) above the active site is disordered in both copies of $C_{modAA}$, which suggests flexibility in this region (Figure 3A).

We combined the structure of $C_{modAA}$ with coevolutionary analysis and modeling to investigate potential interactions with its donor and acceptor T domains. For coevolutionary analysis of $T_1$ and $C_{modAA}$, we extracted 1,534 T:$C_{modAA}$ pairs in which T and $C_{modAA}$ are present within the same protein and separated by 100 or fewer residues. These T:$C_{modAA}$ pairs were aligned and subject to filtered direct coupling analysis (filterDCA).[25] Evolutionarily conserved contacts identified from DCA were mapped on a homology model of $T_1$ that is positioned at the canonical donor T domain-binding site of $C_{modAA}$.[26] The distances observed between the DCA-predicted T:$C_{modAA}$ pairs support this canonical binding mode between $T_1$ and $C_{modAA}$ (Figure S9C, Table S3). Thus, we used existing T-C structures with *holo* T-domains as a guide to build a model of pre-Ala-AMB-$T_1$ bound to $C_{modAA}$ (Figure 3B). The model shows that pre-Ala-AMB can be positioned at the active site within hydrogen bonding distance of residue H1497 (H**H**XXXDG motif, Figure 3B, Figure S9D). Since donor T domains coevolve with C domains,[18] our co-evolutionary analyses indicate that $T_1$ likely binds $C_{modAA}$ at the position observed for regular and terminal C domains.[26]

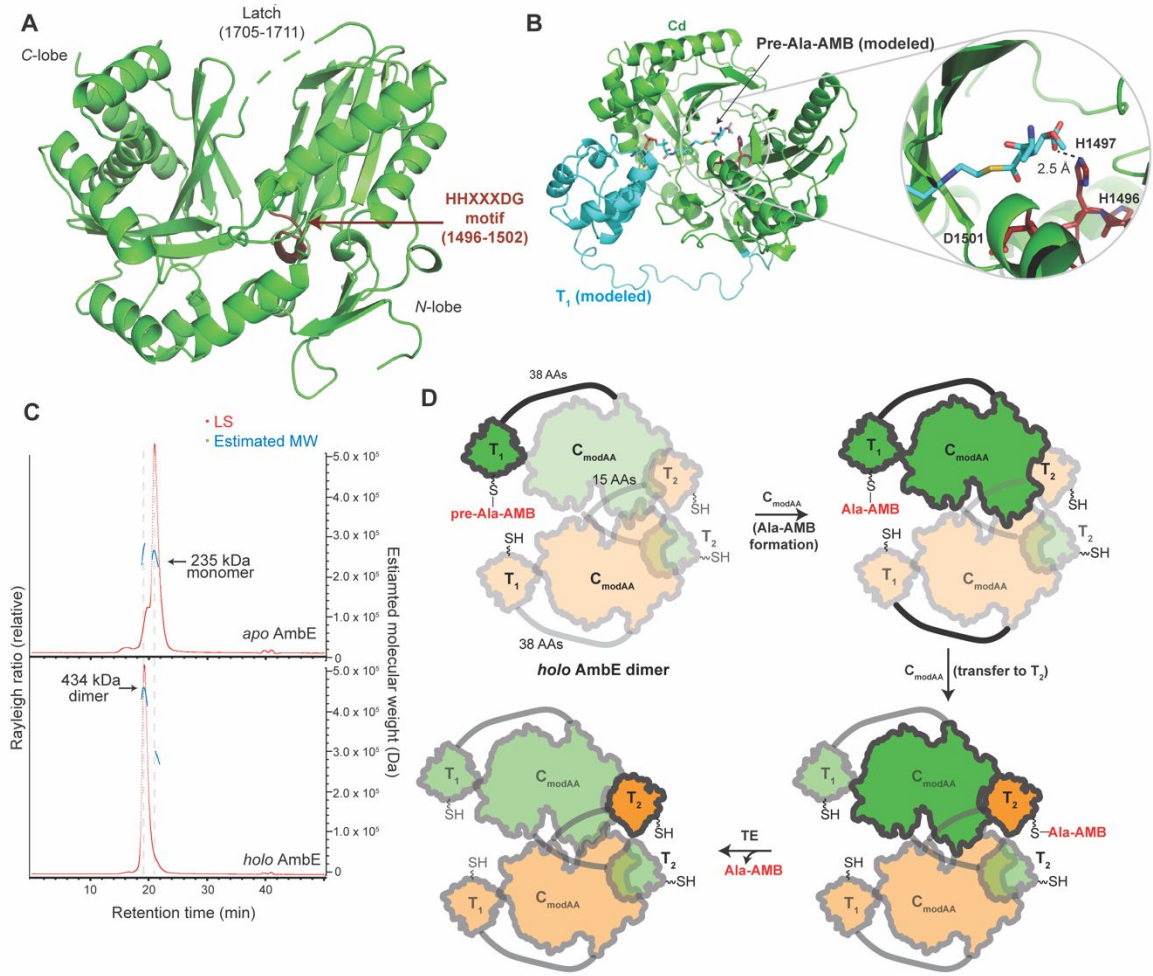


**Figure 3**. Crystal structure of AmbE-$C_{modAA}$ and oligomeric states of full length AmbE. **A**) Overall structure of AmbE-$C_{modAA}$ (PDB: 7R9X) with the active site tunnel between the N- and C-terminal lobes. The conserved HHXXXDG motif is located in the active site tunnel (Figure S9B). **B**) Modeling of pre-Ala-AMB-bound $T_1$ at the canonical donor binding site of $C_{modAA}$ positions pre-Ala-AMB in proximity to the HHXXXDG motif in the active site tunnel. **C**) SEC-MALS analysis shows that *apo* AmbE is a monomer while *holo* AmbE is a dimer. MW, molecular weight. LS, light scattering. **D**) A model for the function of dimeric *holo* AmbE. The $C_{modAA}$ of one AmbE protomer (green) interacts with $T_2$ of the other protomer (orange) as the acceptor T domain.

In contrast, DCA between $C_{modAA}$ and the acceptor $T_2$ failed to give strong signal. Furthermore, when a homology model of $T_2$ is positioned at the acceptor binding site analogous to that previously observed in C domain crystal structures,[26-29] the N terminus of $T_2$ is too far away from the C terminus of $C_{modAA}$: the ~67 Å distance cannot be bridged by the 15-residue linker that exists between $C_{modAA}$ and $T_2$ in AmbE (Figure S10A, left). We attempted to model alternative binding modes of $T_2$ to $C_{modAA}$ where the N terminus of $T_2$ is closer to the C terminus of $C_{modAA}$ for the short $C_{modAA}$-$T_2$ linker to bridge the distance (Figure S10A, middle and right), but there is no position that allows the pantetheine arm to be placed into the canonical acceptor site tunnel. AmbE-$C_{modAA}$ contains an auxiliary opening to the active site (Figure S10B). $T_2$ could bind here between the two central sheets of the CAT folds of each lobe around residues 1582 of the N lobe and 1722 of the C lobe (Figure S10B). This binding mode would be permitted by the 15-residue linker between $C_{modAA}$ and $T_2$; however, it has not been observed in NRPS biology, and

an analogous opening is present in some C domains that are thought to have canonical acceptors (Figure S10C),[30-32] and in the X domain, a non-catalytic C domain family member.[33]

Alternatively, the $C_{modAA}$:$T_2$ linker does not need to bridge the distance between the C terminus of $C_{modAA}$ and N terminus of $T_2$. Should AmbE exist as a homooligomer, $T_2$ from one protomer of AmbE could interact with $C_{modAA}$ from the other. Size exclusion chromatography reveals that purified AmbE contains two species that correspond to a monomer and dimer, with the monomer being the major species. Size exclusion chromatography coupled multi-angle light scattering (SEC-MALS) analysis of the isolated monomer peak in reducing buffer supports the assignment of the monomer (Figure 3C). Incubating the monomer with the phosphopantetheinyl transferase Sfp in the presence of coenzyme A and $MgCl_2$ converts the monomer to the dimer (Figure 3C, S11), suggesting that phosphopantetheinylation by Sfp switches the oligomeric state of AmbE. Indeed, use of the monomeric or dimeric AmbE in a one pot assay shows Ala-AMB production by the dimer but not the monomer (Figure S12). The activity of the dimeric species and inactivity of the monomeric species is consistent with the dimer being *holo* and the monomer being *apo*. $C_{modAA}$ is monomeric in solution and in the crystallized structure, thus, the architecture of the AmbE dimer is unknown. Nonetheless, dimerization of AmbE could permit $C_{modAA}$ to access the canonical acceptor tunnel *in trans* in spite of the short linker between $C_{modAA}$ and $T_2$. To further probe which domains of AmbE are required for dimerization, we also examined the oligomeric states of $C_{modAA}$-$T_2$ and Q-A-MT-$T_1$-$C_{modAA}$. Both constructs exist as monomers regardless of being *apo* or *holo* (Figure S13 and S14A). Furthermore, the S1819A mutant of full length AmbE, which contains a mutation in $T_2$ that prevents phosphopantetheinylation, only exists as a monomer regardless of the *apo*- or *holo*-state of $T_1$ (Figure S14B). Collectively, these results suggest that AmbE dimerization requires *holo* $T_2$ as well as the domains before $C_{modAA}$-$T_2$.

Based on the conversion of pre-Ala-AMB to Ala-AMB on $T_1$, the transfer of Ala-AMB to $T_2$, and the dimeric state of *holo* AmbE, we propose the following steps in late-stage biosynthesis of Ala-AMB (Figure 3D): AmbE-$C_{modAA}$ catalyzes conversion of pre-Ala-AMB to Ala-AMB on $T_1$, followed by the transfer of Ala-AMB from $T_1$ of one AmbE protomer to $T_2$ of the other protomer; then AmbE-TE catalyzes hydrolytic release of Ala-AMB from $T_2$ into solution.

**Mutagenesis of $C_{modAA}$ domain**

We sought to identify important residues for $C_{modAA}$ function by structural modeling, sequence alignment, and mutagenesis. Modeling of $C_{modAA}$ bound to pre-Ala-AMB-$T_1$ and the ppant arm of *holo* $T_2$ positions pre-Ala-AMB in the vicinity of residues H1496, H1497, and D1501 of the HHXXXDG motif [22, 34-35] (Figure 3B, S9D). Sequence alignment of 405 non-identical $C_{modAA}$ domains highlights residues that are mostly conserved within $C_{modAA}$ domains (Figure S15, S16), including R1605, H1632, T1650, and N1700, which are located near the active site (Figure 4A, S17). Several charged residues of AmbE-$C_{modAA}$ that are not conserved in other $C_{modAA}$ domains are also positioned in the active site tunnel, such as D1726, D1728, D1734, and E1736 (Figure 4A, S17). We made a total of 20 mutations to identify residues that are important for AmbE-$C_{modAA}$ activity. These mutations were introduced in full length AmbE to assess how they affected the ability of AmbE to synthesize and release Ala-AMB (Figure 4B). The D1696A and N1700A mutants of AmbE produce Ala-AMB at a higher level than that of wildtype (WT). In contrast, the H1632A and D1726A mutants exhibit lower Ala-AMB production than the WT (Figure 4B). Notably, single mutations in the HHXXXDG motif to Ala (H1496A, H1497A, and D1501A) do not alter Ala-AMB production significantly. However, the H1497A/D1501A double mutation abolishes Ala-AMB production (Figure 4B). LC-MS analysis shows that the AmbE mutants produce a single species of Ala-AMB of the same retention time as the product of the AmbE WT. This observation suggests that all products are in the expected L-Ala-L-AMB configuration and that these mutations do not alter stereochemistry.

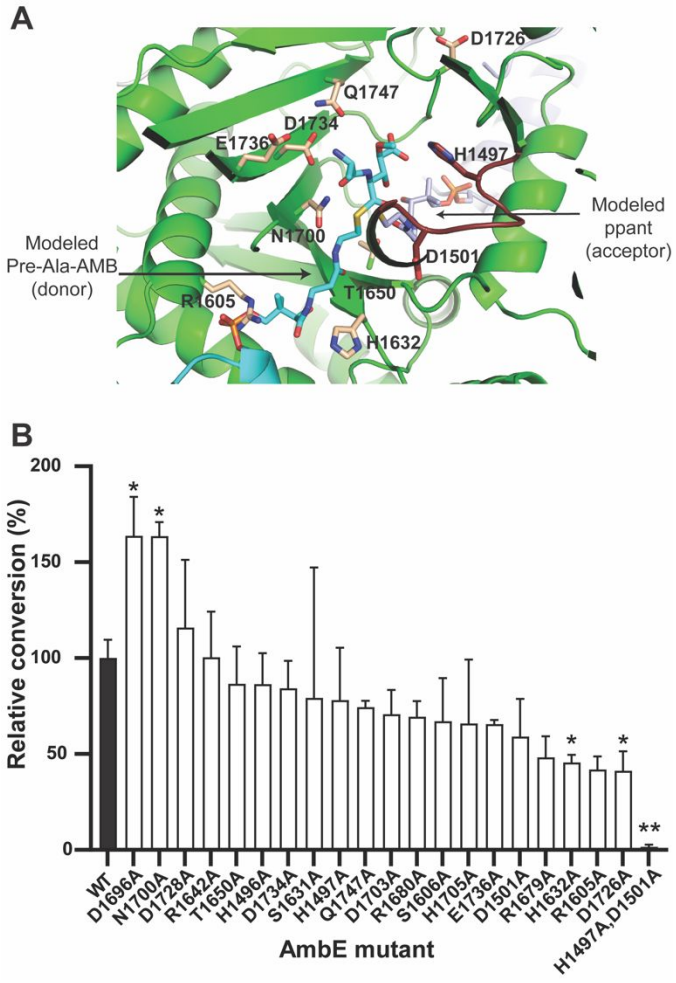


**Figure 4.** Mutagenesis of AmbE-$C_{modAA}$. **A**) Active site of AmbE-$C_{modAA}$ with modeled donor pre-Ala-AMB-ppant and acceptor ppant. **B**) Relative % conversion of Ala to Ala-AMB by full length AmbE WT and mutants. The bar graph depicts the average and standard error of at least two independent replicates for each protein. Statistical tests were performed for each mutant against WT (see methods): *, $p < 0.05$, ** $p < 0.01$.

AMB biosynthesis involves at least ten transformations;[16] we reasoned that the reaction catalyzed by AmbE-$C_{modAA}$ may not be the rate-limiting step and therefore reduction in AmbE-$C_{modAA}$ activity caused by single mutations might not be detected in the one-pot reconstitution assay. Thus, we used the Q-A-MT-$T_1$ and $C_{modAA}$-$T_2$ split system to first accumulate pre-Ala-AMB on Q-A-MT-$T_1$ and then add $C_{modAA}$-$T_2$ to measure the kinetics of $C_{modAA}$-$T_2$ with the goal of directly comparing the rates between WT $C_{modAA}$-$T_2$ and the mutants (Figure 5A). We selected eleven residues of $C_{modAA}$ that are either projected into or located near the active site tunnel for mutation in $C_{modAA}$-$T_2$. Three $C_{modAA}$-$T_2$ mutants, H1496A, D1501A, and D1728A, were insoluble. We purified the other eight $C_{modAA}$-$T_2$ mutants and confirmed that they contain similar secondary structures as the WT by circular dichroism (Figure S18). The relative rates of conversion from pre-Ala-AMB to Ala-AMB catalyzed by WT and mutants of $C_{modAA}$-$T_2$ were obtained (Figure S19 and S20). The T1650A and N1700A mutants of $C_{modAA}$-$T_2$ exhibit increased rates of Ala-AMB formation compared to WT, whereas E1736A shows a similar rate as that of WT (Figure 5B, S20). The Q1747A, D1726A, and R1605A mutations significantly lower the rate of Ala-AMB

formation to 20%, 17%, and 4% of WT, respectively. The H1497A and D1734A mutations abolished Ala-AMB production (Figure 5B, S20).

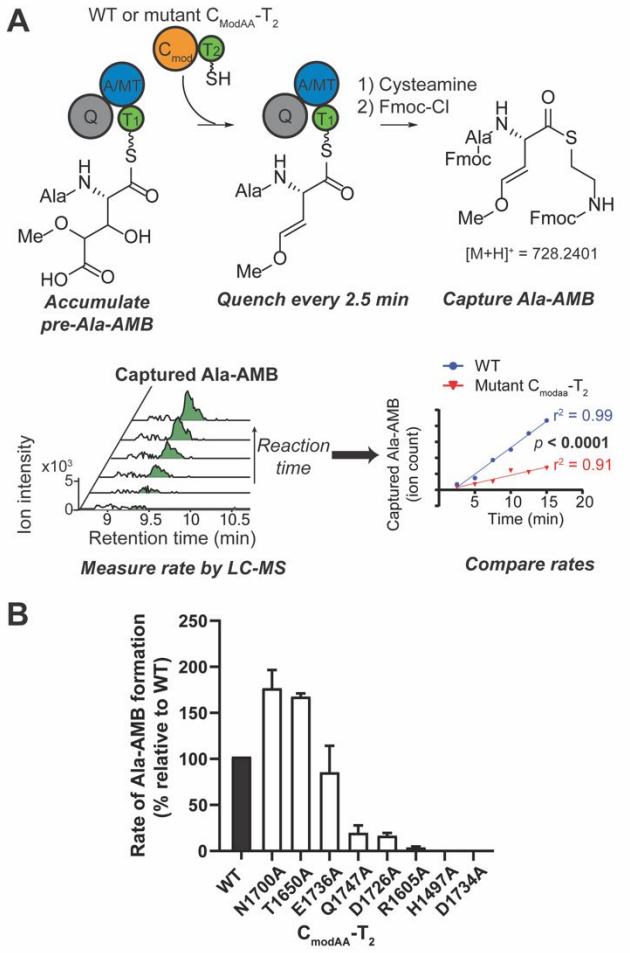


**Figure 5**. Rate analysis of AmbE-$C_{modAA}$-$T_2$ mutants. **A**) Determination of the relative rates of Ala-AMB formation catalyzed by $C_{modAA}$-$T_2$ mutants. Representative graphs comparing the activity of WT $C_{modAA}$-$T_2$ and Q1747A mutant by measuring Ala-AMB formation over time. R sq values for the linear fit are shown for each graph. **B**) Normalized reaction rates of $C_{modAA}$-$T_2$ mutants relative to that of WT. Three independent experiments were performed for each mutant except for R1605A that was tested twice, and error bars depict standard errors of the mean from two or three experiments. Because in every experiment the rate of the WT control is set to 100% for calculation of the relative rate of each mutant, the standard error of the mean for the WT rates is zero. Raw data from each independent experiment are shown in Figure S20 and Table S5. The reaction rates of all mutants except for E1736A are significantly different from that of WT. For each mutant, statistical significance (*p*) was calculated using analysis of covariance to compare the slopes of WT and the mutant in the same experiment (Figure S20).

**Bioinformatic analysis of $C_{modAA}$ domains**

To expand the understanding of $C_{modAA}$ functions in different natural product pathways, we compiled 13 natural products whose biosynthetic gene clusters encode $C_{modAA}$ domains from the MIBiG database (latest version, October 2019).[36] We also curated an additional 7 natural products whose gene clusters contain $C_{modAA}$ domains (Table S4). We proposed the function of

each $C_{modAA}$ domain by correlating the amino acid that we predict based on the specificity of A domain preceding $C_{modAA}$, with the natural product structure, and then cross referenced the proposal with the literature.[9-10, 17, 37] Of the 27 $C_{modAA}$ domains from 20 biosynthetic pathways, 14 $C_{modAA}$ domains from 10 pathways replace a regular C domain and correlate with the incorporation of an upstream Ser or Thr in the precursor and Dha or Dhb in the natural product, respectively, such as microcystin and romidepsin (Figure S1, Figure 6A, 6B).[2-3] This correlation supports a dual role of $C_{modAA}$ domains in dehydrating Ser/Thr to Dha/Dhb and forming the amide bond during peptide elongation. The remaining 10 natural products including AMB do not contain dehydroamino acids (Figure S21). Analysis of their biosynthetic pathways suggests that dehydroamino acid intermediates are further modified via various transformations, including conjugate addition with an amine in prezeamine, pyrrolizidine formation in azabicyclene, and conjugate addition and pyrimidine formation in bleomycin (Figure 6B, Figure S21).[9-10, 38] The $C_{modAA}$-catalyzed dehydration is a central step and unifying theme for these pathways (Figure 6A).

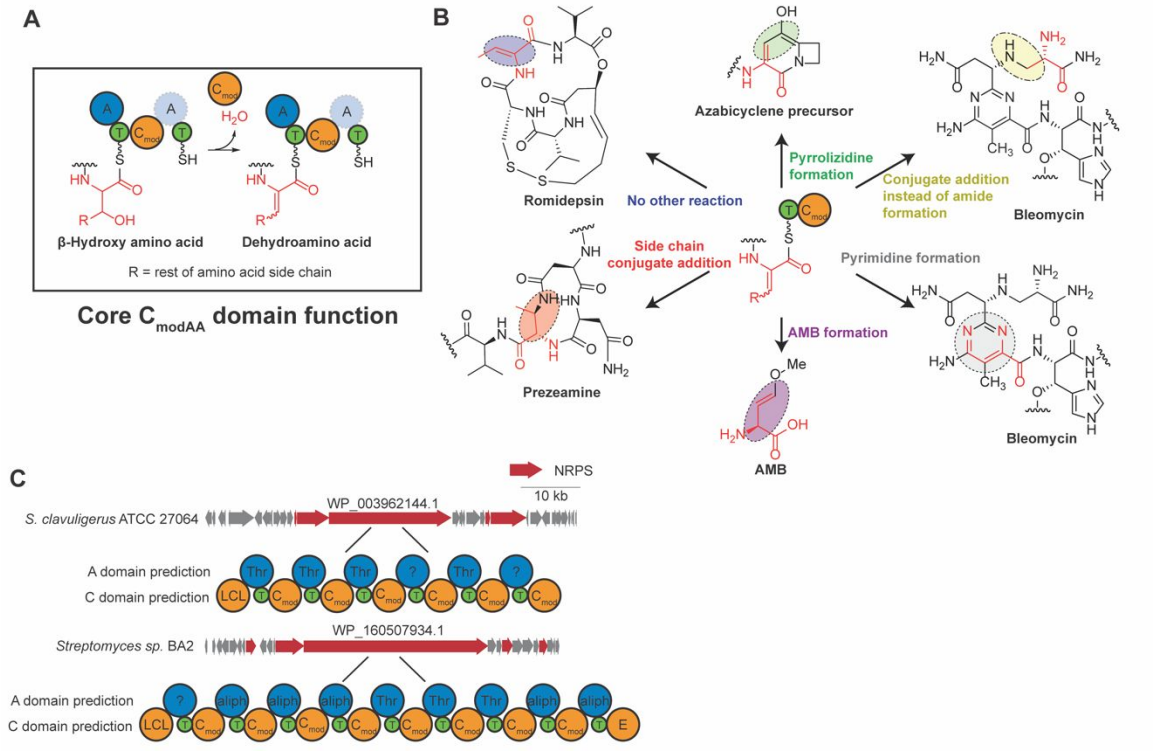


**Figure 6**. Bioinformatic analysis of $C_{modAA}$ domains. **A**) $C_{modAA}$ domains are proposed to catalyze a core dehydration. **B**) Dehydration catalyzed by $C_{modAA}$ domains could enable diverse modifications in nonribosomal peptide biosynthesis. **C**) Uncharacterized biosynthetic gene clusters that contain tandem NRPS modules that harbor $C_{modAA}$ domains.

Phylogenetic analysis of the 27 $C_{modAA}$ domains reveals that some $C_{modAA}$ domains cluster by function (Figure 6B, S22). AmbE-$C_{modAA}$ does not group well with other $C_{modAA}$ domains, which is consistent with its unique dehydrating and decarboxylating function in addition to catalyzing transthioesterification rather than amide bond formation. Nine $C_{modAA}$ domains with additional functions post dehydration form three distinct clades: one clade correlates with pyrimidine formation in the biosynthesis of bleomycin,[9] tallysomycin,[39] and zorbamycin;[40] another clade correlates with conjugate addition instead of amide bond formation in the same biosynthetic pathways; the last clade correlates with pyrrolizidine formation in the biosynthesis of azabicyclene,[10] legonmycin,[41] and brabantamide[42] (Figure S22). The remaining 17 $C_{modAA}$

domains do not form a distinctive group, most of which likely incorporate dehydroamino acids in the natural products via both dehydration of Ser/Thr and amide bond formation. Some of these $C_{modAA}$-installed dehydroamino acids likely undergo further modifications catalyzed by other biosynthetic enzymes.[38, 43-44] Overall, the grouping of $C_{modAA}$ domains does not appear to follow the phylogeny of the producing bacteria, because $C_{modAA}$ domains in the same gene cluster are located in separate clades (e.g. BlmVI and BlmX, Figure S22).

We prospected for novel nonribosomal peptides that may contain dehydroamino acids. We generated a sequence similarity network (SSN)[45] of 4391 putative $C_{modAA}$ domains, which reveals large groups of $C_{modAA}$ domains that are not associated to any known natural products (Figure S23). One notable group harbors several tandem $C_{modAA}$-containing modules in a single NRPS (Figure 6C, Figure S23). The repeat of $C_{modAA}$-containing modules suggests that the products of these NRPSs contain adjacent dehydroamino acids, which are less common in nonribosomal peptides in comparison with RiPPs (Figure S24). Interestingly, although albopeptide contains two adjacent Dha and Dhb, the $C_{modAA}$ domains in its NRPS, AlbB, are located in a different group from the main group that contains tandem $C_{modAA}$ modules in the SSN. Similarly, the $C_{modAA}$ domains in BlmVI and BlmX in bleomycin biosynthesis are located in separate groups in the SSN. These observations corroborate with our phylogenetic analysis that the clustering of $C_{modAA}$ domains does not necessarily follow the phylogeny of the producing bacterial strains. The large number of uncharacterized $C_{modAA}$-containing gene clusters suggests that dehydroamino acids may be much more prevalent in nonribosomal peptides than currently known, which presents a wide and unexplored natural product space that may be accessed using $C_{modAA}$ as a guide.

**Discussion**

We report the biochemical and structural characterization of AmbE-$C_{modAA}$, a member of a major subfamily of C domains with a proposed function in modifying amino acids. We demonstrate that AmbE-$C_{modAA}$ catalyzes dehydrative decarboxylation of pre-Ala-AMB to Ala-AMB. We also provide bioinformatic analysis of 27 different $C_{modAA}$ domains from 20 natural product pathways, which supports a unifying function for $C_{modAA}$ domains in dehydration. Our analysis suggests that $C_{modAA}$ domains either directly incorporate dehydroamino acids into natural products or generate dehydroamino acid intermediates that enable different downstream biosynthetic transformations.

Using AmbE-$C_{modAA}$ as a model to probe $C_{modAA}$ function, we determine that AmbE-$C_{modAA}$ modifies pre-Ala-AMB on the donor $T_1$ domain and transfers the product Ala-AMB to the acceptor $T_2$ domain. Although this conclusion appears contradictory to our previous report that *holo* $T_2$ is required for the production of Ala-AMB,[16] reanalysis of the prior data revealed that the $T_2$ mutant of AmbE generates free Ala-AMB in the presence of cysteamine (Figure S6). This unexpected finding supports the conclusion that $C_{modAA}$ converts pre-Ala-AMB to Ala-AMB on $T_1$. Minimal production of Ala-AMB by the $T_2$ mutant without cysteamine also indicates that transfer of Ala-AMB from $T_1$ to $T_2$ is required for release of Ala-AMB by the TE domain, unless cysteamine is added to offload Ala-AMB from AmbE into solution.

Compared to other subfamilies of C domains that also modify amino acids, including the dual condensation/epimerization domains (dual C/E) and heterocyclization domains (Cy), the timing of $C_{modAA}$ action is reminiscent of dual C/E that catalyzes epimerization on the donor T domain prior to amide bond formation,[46] but distinct from the Cy domain that catalyzes cyclization on the acceptor T domain after amide bond formation.[47-48] The recent report of two $C_{modAA}$ domains from albopeptide biosynthesis also corroborates our finding that $C_{modAA}$ catalyzes dehydration on the donor T domain.[17] Additionally, this work used cysteamine to capture both a Val-Ser dipeptide and a conjugate addition product between cysteamine and Val-Dha dipeptide as biosynthetic intermediates of albopeptide (Val-Dha-Dhb). No conjugate addition products between cysteamine and Dhb were observed in this work,[17] however. Similarly, we could not capture the dehydrated pre-Ala-AMB intermediate before decarboxylation to Ala-AMB despite extensive efforts using AmbE wildtype and mutants, possibly because of the steric hindrance of bulky γ-methoxy glutamate side chain. It is also possible that AmbE-$C_{modAA}$ catalyzes a dehydrative decarboxylation without releasing the dehydroamino acid intermediate, which

remains consistent with the dehydrating function of $C_{modAA}$ domains. Nonetheless, our work and the work on albopeptide use two different systems to provide experimental evidence to support the role of $C_{modAA}$ domains in dehydration and answer the longstanding question on the timing of dehydration.

We obtained the crystal structure of a $C_{modAA}$ domain which reveals a similar overall architecture typical of the C domain family that contains an active site tunnel (Figure S9B).[26] DCA predicts a canonical binding mode of the donor $T_1$ with $C_{modAA}$, but the short 15-residue linker between $C_{modAA}$ and $T_2$ prevents binding of $T_2$ in the canonical acceptor T-binding position.[26] A linker of this length is not unusually short for interdomain linkers in NRPSs, but the lack of an A domain in module 2 of AmbE greatly increases the distance between the acceptor site of $C_{modAA}$ and $T_2$ that this linker would be expected to span. Although it is possible that $T_2$ binds at the end of an auxiliary tunnel in AmbE-$C_{modAA}$ (Figure S10B), it is more likely $T_2$ accesses the canonical tunnel via dimerization (Figure 3D). We show that AmbE dimerizes upon conversion to the *holo* form. Dimerization would allow the ppant arm of $T_2$ in one protomer to enter the canonical acceptor tunnel of the $C_{modAA}$ in the other protomer, which would enable transthioesterification of Ala-AMB from $T_1$ to $T_2$ (Figure 3D). Transferring Ala-AMB to $T_2$ would facilitate hydrolysis catalyzed by the adjacent TE domain, leading to Ala-AMB release (Figure 3D).

Very few NRPS-exclusive systems have been reported to be dimers, including the six-domain vibrobactin synthetase, VibF, and the four-domain saframycin biosynthesis protein, SfmC.[49-50] Two recent dimeric structures of NRPSs reveal dimerization architectures, including the head-to-tail homodimer of the tri-domain, FmoA3, and the depsipeptide synthetase module with an embedded ketoreductase, StsA-AKRT, which dimerizes through a pseudo-$A_{sub}$ domain.[51-52] Our observation of a switch in oligomeric state upon posttranslational phosphopantetheinylation is the first of such report. Phosphopantetheinylation has been shown to promote other interactions, such as between the P450 enzyme NikQ and the NRPS NikP1 in nikkomycin biosynthesis;[53] therefore, self-interaction dependent on the pantetheine arm is not completely without precedence. The requirement of phosphopantetheinylation of $T_2$ for dimerization provides an initial clue for the overall architecture of full length AmbE.

AmbE is not the only NRPS to have a C-T linker of ~15 residues in length. A plot of linker length between C domains immediately followed by T domains (i.e. where the module does not contain an A domain between C and T domains) shows that while the most common linker length is ~50 residues, almost 100 C-T didomains contain fewer than 20 residues in the linker (Figure S25). The longer linkers would be sufficient for T domain binding to the canonical acceptor site (Figure 3B), whereas as our work suggests, the proteins with shorter linkers likely form dimers to allow condensation or transfer to occur. The C-T partial modules can serve unique functions in different biosynthetic pathways, although it is much less common than the canonical C-A-T. For example, the C-T in SyrE is loaded *in trans* by a distal A and T domain and enables peptide extension in syringomycin biosynthesis, whereas both domains of C-T in GliP are required for the cyclization of the diketopiperazine core in gliotoxin biosynthesis.[54-56] Since AmbE-$C_{modAA}$ does not catalyze condensation with an acceptor amino acid, $T_2$ may not be involved in substrate loading or chain extension. Instead, transfer of Ala-AMB to $T_2$ by $C_{modAA}$ may bring Ala-AMB to proximity of the TE domain for hydrolysis.

Based on sequence conservation and residue positioning in the AmbE-$C_{modAA}$ crystal structure, we conducted mutational studies of $C_{modAA}$ in the full length AmbE under multiple turnover conditions and the Q-A-MT-$T_1$/$C_{modAA}$-$T_2$ split system. Single point mutations of full length AmbE do not abolish Ala-AMB production, though the double mutation of H1497A and D1501A abolishes Ala-AMB synthesis, likely due to the collapse of the local fold. Overall, results from the split system show a similar trend to those from full length AmbE, but mutations in the split system exhibit much more profound impacts on activity (Table S6). This phenomenon was also reported for EntF, where mutations introduced in the excised C domain of EntF more significantly impact reaction rates than the same mutations introduced in the full length EntF.[57] The difference between the full length AmbE and the Q-A-MT-$T_1$/$C_{modAA}$-$T_2$ split system may be due to the isolation of the $C_{modAA}$ reaction from the overall AMB biosynthesis that involves at least ten transformations. Alternatively, separation of Q-A-MT-$T_1$ from $C_{modAA}$-$T_2$ could weaken protein-

protein interactions or destabilize the $C_{modAA}$ domain, enhancing the impact of $C_{modAA}$-$T_2$ mutations on reaction rate. Although the activity of split system is less robust than that of full length AmbE, the split system remains functional and has allowed us to measure the rate of catalysis by $C_{modAA}$-$T_2$ under kinetic conditions, which is not possible using full length AmbE. Although $T_2$ is dispensable for the conversion of pre-Ala-AMB to Ala-AMB by Q-A-MT-$T_1$-$C_{modAA}$, the split system requires $C_{modAA}$ to be linked to *holo* $T_2$ for activity. It is possible that *holo* $T_2$ helps stabilize $C_{modAA}$ in the right conformation when $C_{modAA}$ is separated from the rest of AmbE.

We identified four residues that are mostly conserved in $C_{modAA}$ domains and important for activity. These residues, N1700, T1650, R1605, and H1632, are positioned in or near the active site of AmbE-$C_{modAA}$ (Figure 4A). The N1700A mutation both increases the production of Ala-AMB in the full length AmbE assay and increases the rate of Ala-AMB formation in the split system, and T1650A increases the rate of Ala-AMB formation in the split system (Table S6). The increased activity of these mutants could be due to the widening of the $C_{modAA}$ active site through alanine mutation, which suggests a gatekeeping function of N1700 and T1650 (Table S7). The single mutations of conserved $C_{modAA}$ residues that significantly augment activity could inform engineering efforts of other $C_{modAA}$ domains. R1605A mutation decreases the rate of Ala-AMB formation in the split assay (Table S6). The model of $T_1$-$C_{modAA}$ positions R1605 in contact with the phosphoester of the $T_1$ ppant (Figure 4A), hinting at a role in positioning the $T_1$ ppant for proper substrate orientation in the active site (Table S7). H1632 is also located in the modeled donor site of the active site tunnel. Reduced activity of the H1632A mutant of full length AmbE suggests that H1632 may also play a role in substrate positioning (Table S7). D1726 is located on the modeled acceptor $T_2$ domain-side loop of $C_{modAA}$ (Figure 4A) and may help maintain the local fold for interaction with $T_2$ (Table S7). The preponderance of important residues on the side of $C_{modAA}$ where it likely interacts with the donor T domain is consistent with the location of $C_{modAA}$-catalyzed reaction on the donor T domain.

In the HHXXXDG motif, mutation of the first His (H1496) and Asp (D1501) results in insoluble proteins in the $C_{modAA}$-$T_2$ construct, which is consistent with the structural roles that these residues are thought to play in C domain folding.[22, 58] Mutation of the second His (H1497) did not significantly affect the activity of full length AmbE but lowers the reaction rate catalyzed by $C_{modAA}$-$T_2$ to below the detection limit in the split assay (Table S6). This residue is widely accepted as important for positioning the substrate or catalyzing condensation in C domains.[18, 22, 59] Even so, mutation of the second His in C domains in different NRPS pathways exerts different impacts on activity, ranging from completely abolishing activity to causing modest reduction,[34-35, 57-58] which suggests that its role may be compensated by other C domain residues. Similarly, minimal reduction of activity of H1497A in full length AmbE suggests that the role of H1497 is compensated by other residues in AmbE-$C_{modAA}$. D1734 is positioned in the active site and opposite of H1497 (Figure 4A). Like the $C_{modAA}$-$T_2$-H1497A mutant, the $C_{modAA}$-$T_2$-D1734A mutant exhibits no activity in the split system (Table S6). The abolishment of activity suggests that both H1497 and D1734 are essential for activity in the split system. The role of D1734 in substrate positioning remains to determined. The residues E1736 and Q1747 are not conserved in $C_{modAA}$ domains. The comparable rate of the E1736A mutant to that of WT suggests that E1736 is dispensable for $C_{modAA}$-$T_2$ activity. Q1747 is positioned near the opening of the auxiliary tunnel to the active site. While Q1747A mutation lowers the rate of Ala-AMB formation, the role of Q1747 in substrate positioning or local structure is unclear.

Because AmbE-$C_{modAA}$ does not catalyze peptide bond formation, the role of H1497 may involve positioning the pre-Ala-AMB substrate in the AmbE-$C_{modAA}$ active site tunnel or acting as a base that removes the α-proton (Table S7). A similar role has been proposed for the second His in the H**H**XXXDG motif of NocB-$C_5$ domain in nocardicin biosynthesis, a $^{D}C_{L}$ domain distinct from $C_{modAA}$ domains.[18-19] This residue in NocB-$C_5$ is not required for peptide formation but essential for the dehydration of Ser to Dha and subsequent formation of the β-lactam ring.[18-19] Since very few other residues are broadly important for C domain function besides the second His, it is possible that not all dehydrating C domains (NocB-$C_5$ or $C_{modAA}$ domains) use the same mechanism or the same residue as the catalytic base for an E1cb elimination mechanism. Any functional redundancy would also prevent the assignment of a precise residue as the catalytic base. Apart

from dehydration, AmbE-$C_{modAA}$ may catalyze subsequent decarboxylation and isomerization, the latter of which likely requires an active site residue to re-protonate the α-carbon and restore the L-stereochemistry of AMB. The identity of this residue and those involved in in transthioesterification of pre-AMB from $T_1$ and $T_2$ remains to be uncovered.

Besides $C_{modAA}$ domains and NocB-$C_5$, dual C/E domains preceded by A domains that activate β-hydroxy amino acids are also correlated with incorporation of dehydroamino acids,[46] although such activity has not been shown biochemically. Most of these natural products are cyclic lipopeptides isolated from pseudomonads, such as syringomycin,[60] syringopeptin,[61] nunapeptin,[62] and jessenipeptin.[63] Interestingly, the dual C/E domains that correlate with incorporation of Dha/Dhb in these pathways cannot be phylogenetically distinguished from regular dual C/E domains from the same gene clusters (Figure S26A, B). Furthermore, some dual C/E domains preceded by Ser/Thr-activating A domains do not result in the incorporation of Dha/Dhb (Figure S26B). The mechanism of dehydration by dual C/E domains remains to be explored. Compared with dual C/E and $^{D}C_L$ domains that do not typically catalyze dehydration, $C_{modAA}$ domains appear to serve a central dehydrating function that are supported by our biochemical and bioinformatic observations.

In summary, we report the structural and functional interrogation of a dehydrating C domain ($C_{modAA}$) in AMB biosynthesis and begin to shed light on the molecular basis of dehydration in nonribosomal peptides by the $C_{modAA}$ subfamily. Our work provides further bioinformatic evidence to support that $C_{modAA}$ domains perform dehydration as a unifying step in the biosynthesis of therapeutically and ecologically important natural products. Given the diverse chemical and biosynthetic transformations that dehydroamino acids participate in, our discoveries also pave the way for using $C_{modAA}$ domains in natural product diversification, NRPS engineering, and identification of new nonribosomal peptides.

## Materials and Methods

### Purification and Crystallography of AmbE-$C_{modAA}$

Bacterial cultures harboring pLIC-His-AmbE-$C_{modAA}$ were started from a single colony and grown in LB medium that was supplemented with 100 μg/mL ampicillin. A sample of 2 mL starter culture was transferred to a 1 L LB medium that was supplemented with 100 μg/mL ampicillin. The 1 L culture was grown at 37 °C for approximately 4 h until the cell density reached an $OD_{600}$ of 0.5−0.6 when protein expression was induced with 1 mM IPTG. The induced cultures were grown at 16 °C for 16 h, and the bacterial cells were harvested by centrifugation at 6,000 RCF. The cell pellet was resuspended for lysis in Buffer cA (50 mM Tris-Cl, 200 mM NaCl, 10 mM imidazole pH 8.0, 2 mM β-mercaptoethanol (β-ME), pH 7.5) and lysed by sonication. The lysed cells were centrifuged using a JA25.50 rotor at 20,000 RPM for 20 min at 4 °C to remove cell debris. AmbE-$C_{modAA}$ was purified from the supernatant via a 5 mL HiTrap IMAC FF column charged with $Ni^{2+}$. Buffer cA was used as wash buffer, and Buffer cB (50 mM Tris-Cl, 200 mM NaCl, 500 mM imidazole, 2 mM β-ME, pH 7.5) was used as elution buffer over a linear gradient. The eluted sample was then combined, concentrated, and dialyzed overnight with Buffer cC (50 mM Tris-Cl, 50 mM NaCl, 2 mM β-ME, pH 7.5) and digested with His-tagged TEV protease (1 mg per 20 mg of AmbE-$C_{modAA}$) at 4 °C. The digested sample was passed through the HiTrap IMAC FF column again and AmbE-$C_{modAA}$ with the His tag removed was collected in the flowthrough, which was concentrated and separated on a MonoQ HR 16/10 column using Buffer cD (50 mM Tris-Cl, 2 mM β-ME, pH 7.5), buffer cE (50 mM Tris-Cl, 2 mM β-ME, 50 mM NaCl, pH 7.5), and buffer cF (50 mM Tris-Cl, 2 mM β-ME, 1 M NaCl, pH 7.5). Buffer cD was used to equilibrate the column, Buffer cE was used to wash the column after applying the sample, and a linear gradient from Buffer cE to Buffer cF over 100 mL was used to separate AmbE-$C_{modAA}$ from impurities. AmbE-$C_{modAA}$ eluted at ~150 mM NaCl and was concentrated and further purified via a Superdex 200 16/60 column equilibrated with Buffer cG (50 mM Tris-Cl, 200 mM NaCl, 1 mM DTT, pH 7.5). The final purified sample was concentrated, flash frozen at −80 °C, and used for crystallography experiments.

AmbE-$C_{modAA}$ crystallized at a concentration of 10 mg/mL in sitting-well drops after ~5 days at 4 °C using a precipitant solution containing 100 mM bis-Tris propane pH 6.0, 20% polyethylene glycol (PEG) 3350 and 0.2 M sodium iodide. Cryoprotection was performed by dipping the crystal in a solution containing 20% 2-methyl-2,4-pentanediol (MPD), 0.2 M NaCl, 50 mM Tris-Cl pH 7.5, 0.2 M sodium iodide, 20% PEG 3350 and 100 mM bis-Tris propane pH 6.0 before vitrification in liquid nitrogen. The diffraction dataset was collected at the 24-ID-E beamline of the NE-CAT facility at the Advanced Photon Source (APS) in Argonne, Illinois. The data was indexed to I 121 with iMosflm[64] and scaled with AIMLESS on CCP4.[65] The data was phased by PHASER in PHENIX[66] using a homology model of the $C_{modAA}$ domain generated by SWISS-MODEL (separating the N- and C-lobes).[67] The model was refined with COOT[68] and PHENIX refine.[66] There are two copies of AmbE-$C_{modAA}$ in the asymmetric unit.

**One pot assay of Ala-AMB production**

A sample of 7.5 μM AmbB and 7.5 μM AmbE (and AmbE mutants) were incubated with 0.5 μM Sfp (the promiscuous phosphopantetheinyl transferase), 100 μM coenzyme A, 8 mM $MgCl_2$, and 50 mM $KH_2PO_4$ (pH 8.0) at 25 °C for 15 min to reconstitute the *holo* forms of AmbB and AmbE. In a separate reaction vessel, 3.5 μM AmbC and 6.5 μM AmbD were incubated with 100 μM $(NH_4)_2Fe(SO_4)_2$ on ice for 10 min to reconstitute the Fe(II) centers. The AmbB and AmbE reconstitution reaction was mixed with 1 mM L-alanine, 1 mM L-glutamic acid, 1 mM α-KG, 1 mM sodium ascorbate, 1 mM SAM, and 4 mM ATP, as well as AmbC and AmbD reconstituted with Fe(II), which brought the final reaction volume to 50 μL and final concentrations to 7.5 μM AmbB, 3.5 μM AmbC, 6.5 μM AmbD, 7.5 μM AmbE WT or mutants, 0.5 μM Sfp, 100 μM coenzyme A, 8 mM $MgCl_2$, 100 μM $(NH_4)_2Fe(SO_4)_2$, and 50 mM $KH_2PO_4$ (pH 8.0). The assay was incubated at 25 °C for 2 h, quenched with 50 μL of acetonitrile, moved to −20 °C, and incubated for 20 min to precipitate the protein components. The assays were then centrifuged at 14,000 RCF for 5 min to remove the protein precipitates. A 50 μL sample of the quenched reaction supernatant was mixed with 25 μL of 4.5 mg/mL fluorenylmethyloxycarbonyl chloride (Fmoc-Cl) in acetonitrile and 25 μL of 200 mM sodium borate buffer (pH 10.4) for Fmoc-derivatization of the amino acid substrates and the Ala-AMB product. The derivatization reaction was mixed thoroughly for 5 min before it was centrifuged for 5 min at 13,000 RCF.

A 10 μL sample was analyzed using the "general mass spectrometry parameters (supporting information)." Samples were injected onto a Kinetex C18 column (Phenomenex, 50 mm length, 2.6 μm particle size and 100 Å pore size) and separated using the following method at a flow rate of 0.6 mL/min. Solvent A consisted of 0.1% formic acid in water (Fisher Scientific), and solvent B consisted of 0.1% formic acid in acetonitrile (Fisher Scientific). Mobile phase was held at 2% B for 2 min, increased from 2% to 98% B over 10 min in a linear gradient, and held at 98% B for 2 min before returning to 2% B over 1 min. Relative yield was calculated as follows: peak areas in the extracted ion chromatogram that correspond to Fmoc-Ala-AMB (425.1707 $[M+H]^+$ and 447.1527 $[M+Na]^+$) or Fmoc-Ala (312.1230 $[M+H]^+$ and 334.1050 $[M+Na]^+$) were quantified using MassHunter (Agilent). Percent conversion was calculated by dividing the Fmoc-Ala-AMB peak areas by the sum of the Fmoc-Ala and Fmoc-Ala-AMB peak areas. Each reaction for an AmbE mutant was performed 2−5 times along with a reaction for the AmbE WT as a positive control. The mean of percent conversion by the AmbE WT from a total of 23 reactions was set to 100%. Percent conversion by each AmbE mutant was normalized to the mean of the WT, and the relative percent conversion was obtained.

Because the WT and mutant groups are of unequal size (23 vs 2−5, respectively), statistical significance between the WT and mutant activities was analyzed as follows: a Shapiro test shows that WT samples does not follow a normal distribution, but all the mutant samples are normally distributed. All samples have equal variance as determined by Levene test. A *log* transformation of WT and mutant samples yielded normally distributed data. The statistical significance was determined using student's *t* test on the *log* transformed data. We also analyzed the data by directly comparing the WT and each mutant in the same experiments and performing a student's *t* test. This alternative analysis showed that D1726A mutant and the H1497A/D1501A double mutant are significantly different from the WT ($p < 0.05$), although H1632A, N1700A, and

D1696A are not significantly different from the WT controls in the same experiments. The difference from the two statistical analyses suggests systematic errors may exist in the experiments for the one pot assay of full length AmbE H1632A, N1700A, and D1696A mutants. Nonetheless, systematic errors have been taken into account in our kinetic assays of the split system because the $C_{modAA}$-$T_2$ mutant was compared to WT in the same experiments. Overall, single mutations in full length AmbE had modest effect on activity, whereas single mutations in $C_{modAA}$-$T_2$ had a profound impact on activity.

**Kinetic assay of Ala-AMB formation under single turnover conditions**

The one pot reaction for Ala-AMB formation was modified to measure kinetics using the split AmbE-Q-A-MT-$T_1$ and -$C_{modAA}$-$T_2$ system. Two separate initial reactions were prepared, and concentrations of each component varied based on the concentration of stock proteins and are presented as ranges. In one reaction, a sample of AmbB (10.5−11.3 μM) and AmbE-Q-A-MT-$T_1$ (35.1−37.7 μM) were incubated with Sfp (0.35−0.38 μM), coenzyme A (70−80 μM), $MgCl_2$ (5.6−6 mM), and $KH_2PO_4$ (pH 8.0) (35.1−37.7 mM) at 25 °C for 10 min. To this reaction containing Q-A-MT-$T_1$ were added L-alanine (1.4−1.5 mM), L-glutamic acid (1.4−1.5 mM), α-KG (1.4−1.5 mM), sodium ascorbate (1.4−1.5 mM), SAM (1.4−1.5 mM), ATP (5.6−6.0 mM), $(NH_4)_2Fe(SO_4)_2$ (140−150 μM), AmbC (4.9−5.3 μM), and AmbD (9.1−9.7 μM). This reaction mixture was incubated for 45 min at 25 °C. In a separate reaction, AmbE-$C_{modAA}$-$T_2$ WT or mutant (74−87 μM) was incubated with Sfp (0.74−0.87 μM), coenzyme A (150−170 μM), $MgCl_2$ (11.9−13.9 mM), and $KH_2PO_4$ (pH 8.0) (74.4−87 mM) at 25 °C for 45 min to generate *holo* $C_{modAA}$-$T_2$. The reaction mixture containing Q-A-MT-$T_1$ was combined with the $C_{modAA}$-$T_2$-containing reaction to a final volume of 100 μL. The final concentration of each component in the combined reaction was the following: 7.5 μM AmbB, 6.5 μM AmbC, 2.5 μM AmbD, 25 μM Q-A-MT-$T_1$, 25 μM $C_{modAA}$-$T_2$, 100 μM $(NH_4)_2Fe(SO_4)_2$, 0.5 μM Sfp, 100 μM coenzyme A, 1 mM L-alanine, 1 mM L-glutamic acid, 1 mM α-KG, 1 mM sodium ascorbate, 1 mM SAM, 4 mM ATP, 8 mM $MgCl_2$, 50 mM $KH_2PO_4$ potassium phosphate (pH 8.0). Components present in both initial reactions were split equally between both reactions (Sfp, coenzyme A, $KH_2PO_4$ pH 8.0, $MgCl_2$). An aliquot of 15 μL of the combined reaction was transferred to a microcentrifuge tube every 2.5 min up to 15 min and immediately flash-frozen using liquid nitrogen. All the aliquots were immediately quenched using 15 μL acetonitrile upon removal from liquid nitrogen, and cysteamine hydrochloride was added to a concentration of 50 mM. The cysteamine cleavage reactions were mixed at 1,000 RPM at 25 °C for 90 min. After 90 min, samples were moved to −20 °C, and incubated for 20 min to precipitate the protein components. The assays were then centrifuged at 14,000 RCF for 5 min to remove the protein precipitates.

A 25 μL sample of the quenched reaction supernatant was mixed with 180 μL of 2.25 mg/mL Fmoc-Cl in acetonitrile and 50 μL of 200 mM sodium borate buffer (pH 10.4) for Fmoc-derivatization of the cysteamine-captured intermediates. The derivatization reaction was mixed thoroughly for 5 min before it was centrifuged for 5 min at 13,000 RCF. A 10 μL sample was analyzed using “general mass spectrometry methods (supporting information).” Samples were analyzed by LC-MS as described in “one-pot assay of Ala-AMB formation.”

**Size-exclusion chromatography-coupled multi-angle light scattering (SEC-MALS) analysis of *apo*- and *holo*-AmbE**

A sample of 25 μM AmbE was incubated with 0.5 μM Sfp, 100 μM coenzyme A, 1 mM $MgCl_2$, and 50 mM $KH_2PO_4$ (pH 8.0) at 25 °C for 1 h to reconstitute *holo* AmbE. Negative controls lacked coenzyme A, Sfp, or $MgCl_2$, or all three. Reactions were flash frozen in liquid nitrogen and stored at −80 °C until further use. For analysis by SEC-MALS (Wyatt DAWN HELEOS II light scattering instrument interfaced to an Agilent FPLC System equipped with a Superdex 200 Increase 10/300 GL, Wyatt T-rEX refractometer, and Wyatt dynamic light scattering module), 100 μL of each reaction was analyzed by running freshly prepared buffer (50 mM Tris-Cl pH 7.5, 0.5 mM TCEP, 150 mM NaCl, 0.1% w/v sodium azide) over the Superdex column for 50 min at 0.5 mL/min.

**Accession numbers of proteins listed in main text**

AmbB, AAG05693.1 | AmbC, AAG05692.1 | AmbD, AAG05691.1 | AmbE, AAG05690.1 | BlmVI, AAG02359 | BlmX, AAG02355 | AlbB, WP_150244304.1 | NocB, AAT09805.1 | VibF, ABQ21224.1 | SfmC, ABI22133.1| FmoA3, BAP16693.1 | StsA, M5R382.

**Data availability**

Structure coordinates for this study has been deposited in the PDB under the accession code: 7R9X (Supplementary Table 2). All data are published in main text and supporting information. All protein sequences used for bioinformatic analysis are available at 10.5281/zenodo.6536612

**Acknowledgments**

The authors thank Gary Pielak and Emily Patteson for helpful discussion, Qiang Guo for assistance with statistical analysis, Ju-Sung Kim and Ryan Mull for assistance with collecting replicate data, Sheila Podell for manually running NaPDoS on large input files, Angelos Pistofidis for generously providing reagents, and Frank Murphy and Surajit Banerjee (Advanced Photon Source) for facilitating remote collection of diffraction sets. This work was supported by the National Science Foundation (CHE1654678 to BL) and by a CIHR Foundation Grant (FDN-148472) and a Canada Research Chair to TMS. CMF is supported by NSERC MSc and PhD awards and Jon Patteson was supported by UNC Chapel Hill Dissertation Completion Fellowship.

**References**

1. Li, B.; Yu, J. P. J.; Brunzelle, J. S.; Moll, G. N.; van der Donk, W. A.; Nair, S. K., Structure and mechanism of the lantibiotic cyclase involved in nisin biosynthesis. *Science* **2006,** *311* (5766), 1464-1467.
2. Cheng, Y.-q.; Yang, M.; Matter, A. M., Characterization of a gene cluster responsible for the biosynthesis of anticancer agent FK228 in *Chromobacterium violaceum* No. 968. *Appl. Environ. Microbiol.* **2007,** *73*, 3460-3469.
3. Tillett, D.; Dittmann, E.; Erhard, M.; von Döhren, H.; Börner, T.; Neilan, B. A., Structural organization of microcystin biosynthesis in *Microcystis aeruginosa* PCC7806: an integrated peptide–polyketide synthetase system. *Chem. Biol.* **2000,** *7* (10), 753-764.
4. Bogart, J. W.; Bowers, A. A., Dehydroamino acids: chemical multi-tools for late-stage diversification. *Org. Biomol. Chem.* **2019,** *17* (15), 3653-3669.
5. MacKintosh, R. W.; Dalby, K. N.; Campbell, D. G.; Cohen, P. T. W.; Cohen, P.; MacKintosh, C., The cyanobacterial toxin microcystin binds covalently to cysteine-273 on protein phosphatase 1. *FEBS Lett.* **1995,** *371* (3), 236-240.
6. Dadová, J.; Galan, S. R. G.; Davis, B. G., Synthesis of modified proteins via functionalization of dehydroalanine. *Curr. Opin. Chem. Biol.* **2018,** *46*, 71-81.
7. Repka, L. M.; Chekan, J. R.; Nair, S. K.; van der Donk, W. A., Mechanistic understanding of lanthipeptide biosynthetic enzymes. *Chem. Rev.* **2017,** *117* (8), 5457-5520.
8. Arnison, P. G.; Bibb, M. J.; Bierbaum, G.; Bowers, A. A.; Bugni, T. S.; Bulaj, G.; Camarero, J. A.; Campopiano, D. J.; Challis, G. L.; Clardy, J., et al., Ribosomally synthesized and post-translationally modified peptide natural products: overview and recommendations for a universal nomenclature. *Nat. Prod. Rep.* **2013,** *30* (1), 108-160.
9. Du, L.; Sánchez, C.; Chen, M.; Edwards, D. J.; Shen, B., The biosynthetic gene cluster for the antitumor drug bleomycin from *Streptomyces verticillus* ATCC15003 supporting functional interactions between nonribosomal peptide synthetases and a polyketide synthase. *Chem. Biol.* **2000,** *7* (8), 623-642.
10. Patteson, J. B.; Lescallette, A. R.; Li, B., Discovery and biosynthesis of azabicyclene, a conserved nonribosomal peptide in *Pseudomonas aeruginosa*. *Org. Lett.* **2019,** *21* (13), 4955-4959.

11. Walsh, C. T., Insights into the chemical logic and enzymatic machinery of NRPS assembly lines. *Nat. Prod. Rep.* **2016,** *33* (2), 127-135.
12. Süssmuth, R. D.; Mainz, A., Nonribosomal peptide synthesis—principles and prospects. *Angew. Chem. Int. Ed.* **2017,** *56* (14), 3770-3821.
13. Challis, G. L.; Ravel, J.; Townsend, C. A., Predictive, structure-based model of amino acid recognition by nonribosomal peptide synthetase adenylation domains. *Chem. Biol.* **2000,** *7* (3), 211-224.
14. Stachelhaus, T.; Mootz, H. D.; Marahiel, M. A., The specificity-conferring code of adenylation domains in nonribosomal peptide synthetases. *Chem. Biol.* **1999,** *6* (8), 493-505.
15. Ziemert, N.; Podell, S.; Penn, K.; Badger, J. H.; Allen, E.; Jensen, P. R., The natural product domain seeker NaPDoS: A phylogeny based bioinformatic tool to classify secondary metabolite gene diversity. *PLoS One* **2012,** *7*, 1-9.
16. Patteson, J. B.; Dunn, Z. D.; Li, B., In vitro biosynthesis of the nonproteinogenic amino acid methoxyvinylglycine. *Angew. Chem. Int. Ed.* **2018,** *57*, 6780-6785.
17. Wang, S.; Fang, Q.; Lu, Z.; Gao, Y.; Trembleau, L.; Ebel, R.; Andersen, J. H.; Philips, C.; Law, S.; Deng, H., Discovery and biosynthetic investigation of a new antibacterial dehydrated non-ribosomal tripeptide. *Angew. Chem. Int. Ed.* **2021,** *60* (6), 3229-3237.
18. Wheadon, M. J.; Townsend, C. A., Evolutionary and functional analysis of an NRPS condensation domain integrates β-lactam, D-amino acid, and dehydroamino acid synthesis. *Proc. Natl. Acad. Sci. U. S. A.* **2021,** *118* (17), e2026017118.
19. Long, D. H.; Townsend, C. A., Acyl donor stringency and dehydroaminoacyl intermediates in β-lactam formation by a non-ribosomal peptide synthetase. *ACS Chem. Biol.* **2021,** *16* (5), 806-812.
20. Chahtane, H.; Nogueira Füller, T.; Allard, P.-M.; Marcourt, L.; Ferreira Queiroz, E.; Shanmugabalaji, V.; Falquet, J.; Wolfender, J.-L.; Lopez-Molina, L., The plant pathogen *Pseudomonas aeruginosa* triggers a DELLA-dependent seed germination arrest in *Arabidopsis*. *eLife* **2018,** *7*, e37082.
21. Belecki, K.; Townsend, C. A., Biochemical determination of enzyme-bound metabolites: preferential accumulation of a programmed octaketide on the enediyne polyketide synthase CalE8. *J. Am. Chem. Soc.* **2013,** *135* (38), 14339-14348.
22. Bloudoff, K.; Schmeing, T. M., Structural and functional aspects of the nonribosomal peptide synthetase condensation domain superfamily: discovery, dissection and diversity. *Biochim. Biophys. Acta, Proteins Proteomics* **2017,** *1865* (11, Part B), 1587-1604.
23. Bloudoff, K.; Rodionov, D.; Schmeing, T. M., Crystal structures of the first condensation domain of CDA synthetase suggest conformational changes during the synthetic cycle of nonribosomal peptide synthetases. *J. Mol. Biol.* **2013,** *425* (17), 3137-3150.
24. Izoré, T.; Candace Ho, Y. T.; Kaczmarski, J. A.; Gavriilidou, A.; Chow, K. H.; Steer, D. L.; Goode, R. J. A.; Schittenhelm, R. B.; Tailhades, J.; Tosin, M., et al., Structures of a non-ribosomal peptide synthetase condensation domain suggest the basis of substrate selectivity. *Nat. Commun.* **2021,** *12* (1), 2511.
25. Muscat, M.; Croce, G.; Sarti, E.; Weigt, M., FilterDCA: Interpretable supervised contact prediction using inter-domain coevolution. *PLoS Comput. Biol.* **2020,** *16* (10), e1007621.
26. Reimer, J. M.; Eivaskhani, M.; Harb, I.; Guarné, A.; Weigt, M.; Schmeing, T. M., Structures of a dimodular nonribosomal peptide synthetase reveal conformational flexibility. *Science* **2019,** *366* (6466), eaaw4388.
27. Tanovic, A.; Samel, S. A.; Essen, L.-O.; Marahiel, M. A., Crystal structure of the termination module of a nonribosomal peptide synthetase. *Science* **2008,** *321* (5889), 659-663.
28. Kreitler, D. F.; Gemmell, E. M.; Schaffer, J. E.; Wencewicz, T. A.; Gulick, A. M., The structural basis of *N*-acyl-α-amino-β-lactone formation catalyzed by a nonribosomal peptide synthetase. *Nat. Commun.* **2019,** *10* (1), 3432.
29. Drake, E. J.; Miller, B. R.; Shi, C.; Tarrasch, J. T.; Sundlov, J. A.; Allen, C. L.; Skiniotis, G.; Aldrich, C. C.; Gulick, A. M., Structures of two distinct conformations of holo-non-ribosomal peptide synthetases. *Nature* **2016,** *529* (7585), 235-8.

30. Miller, B. R.; Drake, E. J.; Shi, C.; Aldrich, C. C.; Gulick, A. M., Structures of a nonribosomal peptide synthetase module bound to MbtH-like proteins support a highly dynamic domain architecture. *J. Biol. Chem.* **2016,** *291* (43), 22559-22571.
31. Tarry, M. J.; Haque, A. S.; Bui, K. H.; Schmeing, T. M., X-ray crystallography and electron microscopy of cross- and multi-module nonribosomal peptide synthetase proteins reveal a flexible architecture. *Structure* **2017,** *25* (5), 783-793.
32. Tan, K.; Zhou, M.; Jedrzejczak, R. P.; Wu, R.; Higuera, R. A.; Borek, D.; Babnigg, G.; Joachimiak, A., Structures of teixobactin-producing nonribosomal peptide synthetase condensation and adenylation domains. *Curr. Res. Struct. Biol.* **2020,** *2*, 14-24.
33. Haslinger, K.; Peschke, M.; Brieke, C.; Maximowitsch, E.; Cryle, M. J., X-domain of peptide synthetases recruits oxygenases crucial for glycopeptide biosynthesis. *Nature* **2015,** *521* (7550), 105-109.
34. Keating, T. A.; Marshall, C. G.; Walsh, C. T.; Keating, A. E., The structure of VibH represents nonribosomal peptide synthetase condensation, cyclization and epimerization domains. *Nat. Struct. Biol.* **2002,** *9* (7), 522-526.
35. Bergendahl, V.; Linne, U.; Marahiel, M. A., Mutational analysis of the C-domain in nonribosomal peptide synthesis. *Eur. J. Biochem.* **2002,** *269* (2), 620-629.
36. Medema, M. H.; Kottmann, R.; Yilmaz, P.; Cummings, M.; Biggins, J. B.; Blin, K.; de Bruijn, I.; Chooi, Y. H.; Claesen, J.; Coates, R. C., et al., Minimum information about a biosynthetic gene cluster. *Nat. Chem. Biol.* **2015,** *11*, 625-631.
37. Johnston, C. W.; Zvanych, R.; Khyzha, N.; Magarvey, N. A., Nonribosomal assembly of natural lipocyclocarbamate lipoprotein-associated phospholipase inhibitors. *ChemBioChem* **2013,** *14*, 431-435.
38. Masschelein, J.; Clauwers, C.; Awodi, U. R.; Stalmans, K.; Vermaelen, W.; Lescrinier, E.; Aertsen, A.; Michiels, C.; Challis, G. L.; Lavigne, R., A combination of polyunsaturated fatty acid, nonribosomal peptide and polyketide biosynthetic machinery is used to assemble the zeamine antibiotics. *Chem. Sci.* **2015,** *6*, 923-929.
39. Tao, M.; Wang, L.; Wendt-Pienkowski, E.; George, N. P.; Galm, U.; Zhang, G.; Coughlin, J. M.; Shen, B., The tallysomycin biosynthetic gene cluster from *Streptoalloteichus hindustanus* E465-94 ATCC 31158 unveiling new insights into the biosynthesis of the bleomycin family of antitumor antibiotics. *Mol. Biosyst.* **2007,** *3* (1), 60-74.
40. Galm, U.; Wendt-Pienkowski, E.; Wang, L.; George, N. P.; Oh, T.-J.; Yi, F.; Tao, M.; Coughlin, J. M.; Shen, B., The biosynthetic gene cluster of zorbamycin, a member of the bleomycin family of antitumor antibiotics, from *Streptomyces flavoviridis* ATCC 21892. *Mol. Biosyst.* **2009,** *5* (1), 77-90.
41. Huang, S.; Tabudravu, J.; Elsayed, S. S.; Travert, J.; Peace, D.; Tong, M. H.; Kyeremeh, K.; Kelly, S. M.; Trembleau, L.; Ebel, R., et al., Discovery of a single monooxygenase that catalyzes carbamate formation and ring contraction in the biosynthesis of the legonmycins. *Angew. Chem. Int. Ed.* **2015,** *54*, 12697-12701.
42. Schmidt, Y.; van der Voort, M.; Crüsemann, M.; Piel, J.; Josten, M.; Sahl, H.-G.; Miess, H.; Raaijmakers, J. M.; Gross, H., Biosynthetic origin of the antibiotic cyclocarbamate brabantamide A (SB-253514) in plant-associated *Pseudomonas*. *ChemBioChem* **2014,** *15* (2), 259-266.
43. Mori, T.; Cahn, J. K. B.; Wilson, M. C.; Meoded, R. A.; Wiebach, V.; Martinez, A. F. C.; Helfrich, E. J. N.; Albersmeier, A.; Wibberg, D.; Dätwyler, S., et al., Single-bacterial genomics validates rich and varied specialized metabolism of uncultivated *Entotheonella* sponge symbionts. *Proc. Natl. Acad. Sci. U. S. A.* **2018,** *115* (8), 1718-1723.
44. Fuchs, S. W.; Grundmann, F.; Kurz, M.; Kaiser, M.; Bode, H. B., Fabclavines: bioactive peptide–polyketide-polyamino hybrids from *Xenorhabdus*. *ChemBioChem* **2014,** *15* (4), 512-516.
45. Zallot, R.; Oberg, N.; Gerlt, J. A., The EFI web resource for genomic enzymology tools: Leveraging protein, genome, and metagenome databases to discover novel enzymes and metabolic pathways. *Biochemistry* **2019,** *58* (41), 4169-4182.

46. Balibar, C. J.; Vaillancourt, F. H.; Walsh, C. T., Generation of D amino acid residues in assembly of arthrofactin by dual condensation/epimerization domains. *Chem. Biol.* **2005,** *12* (11), 1189-1200.
47. Bloudoff, K.; Fage, C. D.; Marahiel, M. A.; Schmeing, T. M., Structural and mutational analysis of the nonribosomal peptide synthetase heterocyclization domain provides insight into catalysis. *Proc. Natl. Acad. Sci. U. S. A.* **2017,** *114*, 95-100.
48. Luo, L.; Kohli, R. M.; Onishi, M.; Linne, U.; Marahiel, M. a.; Walsh, C. T., Timing of epimerization and condensation reactions in nonribosomal peptide assembly lines: Kinetic analysis of phenylalanine activating elongation modules of tyrocidine synthetase B. *Biochemistry* **2002,** *41*, 9184-9196.
49. Hillson, N. J.; Balibar, C. J.; Walsh, C. T., Catalytically inactive condensation domain C1 is responsible for the dimerization of the VibF subunit of vibriobactin synthetase. *Biochemistry* **2004,** *43* (35), 11344-51.
50. Koketsu, K.; Watanabe, K.; Suda, H.; Oguri, H.; Oikawa, H., Reconstruction of the saframycin core scaffold defines dual Pictet-Spengler mechanisms. *Nat. Chem. Biol.* **2010,** *6* (6), 408-410.
51. Katsuyama, Y.; Sone, K.; Harada, A.; Kawai, S.; Urano, N.; Adachi, N.; Moriya, T.; Kawasaki, M.; Shin-ya, K.; Senda, T., et al., Structural and functional analyses of the tridomain-nonribosomal peptide synthetase FmoA3 for 4-methyloxazoline ring formation. *Angew. Chem. Int. Ed.* **2021,** *60* (26), 14554-14562.
52. Alonzo, D. A.; Chiche-Lapierre, C.; Tarry, M. J.; Wang, J.; Schmeing, T. M., Structural basis of keto acid utilization in nonribosomal depsipeptide synthesis. *Nat. Chem. Biol.* **2020,** *16* (5), 493-496.
53. Wise, C. E.; Makris, T. M., Recruitment and regulation of the non-ribosomal peptide synthetase modifying cytochrome P450 involved in nikkomycin biosynthesis. *ACS Chem. Biol.* **2017,** *12* (5), 1316-1326.
54. Singh, G. M.; Vaillancourt, F. H.; Yin, J.; Walsh, C. T., Characterization of SyrC, an aminoacyltransferase shuttling threonyl and chlorothreonyl residues in the syringomycin biosynthetic assembly line. *Chem. Biol.* **2007,** *14* (1), 31-40.
55. Balibar, C. J.; Walsh, C. T., GliP, a multimodular nonribosomal peptide synthetase in *Aspergillus fumigatus*, makes the diketopiperazine scaffold of gliotoxin. *Biochemistry* **2006,** *45* (50), 15029-15038.
56. Baccile, J. A.; Le, H. H.; Pfannenstiel, B. T.; Bok, J. W.; Gomez, C.; Brandenburger, E.; Hoffmeister, D.; Keller, N. P.; Schroeder, F. C., Diketopiperazine formation in fungi requires dedicated cyclization and thiolation domains. *Angew. Chem. Int. Ed.* **2019,** *58* (41), 14589-14593.
57. Roche, E. D.; Walsh, C. T., Dissection of the EntF condensation domain boundary and active site residues in nonribosomal peptide synthesis. *Biochemistry* **2003,** *42* (5), 1334-1344.
58. Stachelhaus, T.; Walsh, C. T., Mutational analysis of the epimerization domain in the initiation module PheATE of gramicidin S synthetase. *Biochemistry* **2000,** *39* (19), 5775-5787.
59. Bloudoff, K.; Alonzo, Diego A.; Schmeing, T. M., Chemical probes allow structural insight into the condensation reaction of nonribosomal peptide synthetases. *Cell Chem. Biol.* **2016,** *23* (3), 331-339.
60. Fukuchi, N.; Isogai, A.; Nakayama, J.; Takayama, S.; Yamashita, S.; Suyama, K.; Takemoto, J. Y.; Suzuki, A., Structure and stereochemistry of three phytotoxins, syringomycin, syringotoxin and syringostatin, produced by pseudomonas syringae pv. syringae. *J. Chem. Soc., Perkin Trans. 1* **1992,** (9), 1149-1157.
61. Ballio, A.; Barra, D.; Bossa, F.; Collina, A.; Grgurina, I.; Marino, G.; Moneti, G.; Paci, M.; Pucci, P.; Segre, A., et al., Syringopeptins, new phytotoxic lipodepsipeptides of Pseudomonas syringae pv. syringae. *FEBS Lett.* **1991,** *291* (1), 109-112.
62. Michelsen Charlotte, F.; Watrous, J.; Glaring Mikkel, A.; Kersten, R.; Koyama, N.; Dorrestein Pieter, C.; Stougaard, P.; Greenberg, E. P., Nonribosomal peptides, key biocontrol components for *Pseudomonas fluorescens* In5, isolated from a greenlandic suppressive soil. *mBio 6* (2), e00079-15.

63. Arp, J.; Götze, S.; Mukherji, R.; Mattern, D. J.; García-Altares, M.; Klapper, M.; Brock, D. A.; Brakhage, A. A.; Strassmann, J. E.; Queller, D. C., et al., Synergistic activity of cosecreted natural products from amoebae-associated bacteria. *Proc. Natl. Acad. Sci. U. S. A.* **2018,** *115* (15), 3758.
64. Leslie, A. G. W.; Powell, H. R. In *Processing diffraction data with mosflm*, Evolving Methods for Macromolecular Crystallography, Dordrecht, 2007//; Read, R. J.; Sussman, J. L., Eds. Springer Netherlands: Dordrecht, 2007; pp 41-51.
65. Evans, P. R.; Murshudov, G. N., How good are my data and what is the resolution? *Acta Crystallogr., Sect. D: Biol. Crystallogr.* **2013,** *69* (Pt 7), 1204-1214.
66. Adams, P. D.; Afonine, P. V.; Bunkóczi, G.; Chen, V. B.; Davis, I. W.; Echols, N.; Headd, J. J.; Hung, L.-W.; Kapral, G. J.; Grosse-Kunstleve, R. W., et al., PHENIX: a comprehensive Python-based system for macromolecular structure solution. *Acta Crystallogr., Sect. D: Biol. Crystallogr.* **2010,** *66* (Pt 2), 213-221.
67. Waterhouse, A.; Bertoni, M.; Bienert, S.; Studer, G.; Tauriello, G.; Gumienny, R.; Heer, F. T.; de Beer, T. A. P.; Rempfer, C.; Bordoli, L., et al., SWISS-MODEL: homology modelling of protein structures and complexes. *Nucleic Acids Res.* **2018,** *46* (W1), W296-W303.
68. Emsley, P.; Lohkamp, B.; Scott, W. G.; Cowtan, K., Features and development of Coot. *Acta Crystallogr., Sect. D: Biol. Crystallogr.* **2010,** *66* (Pt 4), 486-501.

TOC Graphic

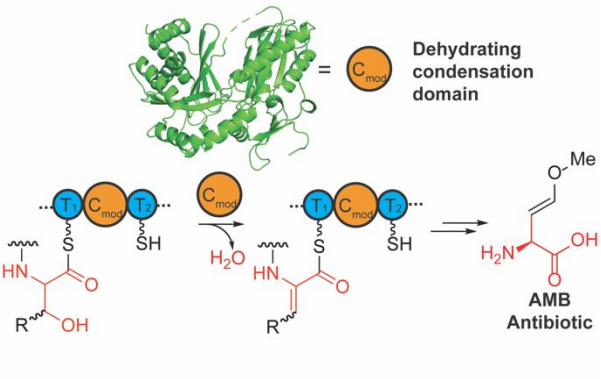


Supporting information: materials, additional experimental procedures, tables and supplementary figures, including mass spectrometry, crystallographic, bioinformatic, and protein purity data.